

Dual-polarization lidar using a liquid crystal variable retarder

Nathan L. Seldomridge

Joseph A. Shaw, MEMBER SPIE

Kevin S. Repasky

Montana State University

Electrical and Computer Engineering

Department

Cobleigh 610

Bozeman, Montana 59717

E-mail: jshaw@ece.montana.edu

Abstract. We describe the design and characterization of a compact dual-polarization lidar that uses a liquid crystal variable retarder (LCVR) to discriminate between backscattered polarization states on alternate laser pulses (at 30 Hz). Measurements of the polarization discrimination of the system, including the liquid crystal and a Schmidt-Cassegrain receiver telescope, show that depolarization ratios can be determined with an additive error of less than 0.4%. The source is a Nd:YAG laser with a wavelength of 532 nm, pulse energy of 118 mJ, and pulse-repetition frequency of 30 Hz. The normal operating range is 15 km, with a 1.5-m range resolution. The full-angle receiver field of view is variable up to 8.8 mrad. Sample data from atmospheric clouds demonstrate the use of lidar depolarization measurements for distinguishing between ice and liquid water in thin clouds with low multiple scattering (with cloud phase verified using radiosonde profiles of atmospheric temperature and humidity). Also shown is a lidar observation of a depolarizing layer over Bozeman, Montana, identified as subvisual cirrus, aerosols transported from in or near China, or a combination thereof. © 2006 Society of Photo-Optical Instrumentation Engineers. [DOI: 10.1117/1.2358636]

Subject terms: lidar; liquid crystals; polarization; clouds; aerosols; Asian dust.

Paper 050590RR received Jul. 20, 2005; revised manuscript received Feb. 6, 2006; accepted for publication Mar. 28, 2006; published online Oct. 10, 2006. This paper is a revision of a paper presented at the SPIE conference on Polarization Science and Remote Sensing II, Aug. 2005, San Diego, California. The paper presented there appears (unrefereed) in SPIE proceedings Vol. 5888.

1 Introduction

Sensing the polarization of backscattered light can enhance lidar measurements by providing additional information beyond signal strength and timing. Cloud lidar systems use polarization sensitivity to distinguish between ice and water in clouds, since the backscattered laser light is more depolarized by scattering from polyhedral ice crystals than by spherical water droplets.¹ Polarization sensitivity also is useful in lidar measurements of aerosols,² vegetation,³ soils,⁴ fish,⁵ and insects.⁶ The lidar systems developed for these various applications use different mechanisms to provide polarization discrimination, generally falling into categories of either single detector with time-sequential polarization switching or dual detectors with simultaneous dual-polarization detection. The former has the advantages of requiring fewer receiver components and offering simpler single-detector calibration, while the latter has the advantage of simultaneous polarization data acquisition, which can be particularly helpful with rapidly changing scenes or moving objects.

In this paper, we describe a lidar system developed for dual-polarization measurements in a wide range of applications, including, but not limited to, cloud measurements.⁷ The lidar uses a single detector and a liquid crystal variable retarder (LCVR) to achieve shot-to-shot polarization discrimination. The system has been characterized and its polarization-sensing performance demonstrated with mea-

surements of atmospheric clouds and aerosols. After briefly explaining the background of the dual-polarization cloud lidar as for those readers who are interested in the dual-polarization lidar but lack experience with cloud-lidar data, we describe the lidar system, explain the procedure and results of the characterization of its polarization sensitivity, and show sample data for clouds and atmospheric aerosols. The focus in this paper is on the choice and capabilities of the liquid crystal variable retarder in the lidar receiver to measure different polarization states. We quantify the lidar polarization accuracy with laboratory measurements, especially characterizing the effect of the liquid crystal and the reflective telescope. The depolarization measurement capability is demonstrated by discrimination of ice and liquid clouds, with validation from radiosonde profiles of atmospheric temperature and humidity.

2 Background

One of many useful applications of a dual-polarization lidar is to measure the optical properties of aerosols and clouds in the atmosphere for studying weather and climate. The radiative properties of clouds and aerosols, along with those of water vapor, are some of the most important factors in the heat budget and climate of the Earth.⁸ The effects of clouds depend on the ice or water particle shapes, sizes, and concentrations and on the vertical position of the cloud in the atmosphere. These parameters help determine whether the cloud contributes a net warming or cooling effect, largely determined by the cloud transmittances for

short-wave and long-wave energy. Liquid-water clouds are often optically thick and tend to have a net cooling influence because the low short-wave transmission ultimately reduces the surface heating. Conversely, cirrus clouds tend to be much less optically dense⁹ but often have a net warming effect on the Earth-atmosphere system. If the water has not frozen by other processes, it does so by homogeneous nucleation at approximately -40°C , leaving clouds that are composed exclusively of ice crystals.¹⁰ Thin “subvisual” cirrus also presumably has a similar effect on the climate but can be easily missed in satellite imagery. Mixed-phase clouds, in which ice and liquid water coexist, further complicate these issues.

Natural and anthropogenic aerosols also affect climate strongly. Aerosols can have a direct radiative effect on climate, by absorption or scattering, or they may have an indirect effect, by acting as condensation or deposition nuclei for the formation of clouds.¹¹ A lidar is well suited for measuring optical properties that can be used to retrieve particle vertical distributions and microphysical properties, especially in combination with other sensors such as radiometers, imagers, and radars.

Our dual-polarization lidar detects the backscattered light in two orthogonal linear polarization channels, measured with respect to the source, which are termed “co-polarized” (co-pol; parallel) and “cross-polarized” (cross-pol; orthogonal). The added capability of a dual-polarization lidar over a conventional lidar is that a comparison of the co-pol and cross-pol signals can be used to distinguish between spherical and nonspherical scattering particles.

Such a comparison employs the depolarization ratio δ , the ratio of the received cross-polarized and co-polarized signals (P_{\perp} and P_{\parallel} and, respectively). For a system with polarization-insensitive transmitter optics, this is the same as the ratio of backscattering cross sections per unit volume for each polarization (β_{\perp} and β_{\parallel}). All else in the lidar equation cancels out in the ratio, except for presumably negligible atmospheric transmission differences, so the depolarization ratio can be ascribed directly to particle scattering properties¹²:

$$\delta(r) = \frac{P_{\perp}(r)}{P_{\parallel}(r)} = \frac{\beta_{\perp}(r)}{\beta_{\parallel}(r)}. \quad (1)$$

When applied to clouds, dual polarization allows discrimination between quasi-spherical liquid cloud droplets and nonspherical ice crystals. For single scattering, Liou and Lahore¹³ found that most of the backscattered energy from a group of randomly oriented hexagonal plates or columns is the result of precisely two internal reflections. In contrast, for a spherical water droplet, the backscatter is primarily the result of an edge ray, which travels by surface waves, although a small contribution comes from a central ray.

For a fixed laser source polarization, the polarization of the backscattered light (which is the result of a transmission, two reflections, and another transmission) depends on the ice crystal orientation. It is best not to think of an ice crystal as *changing* the incident polarization state so much as it *differentially backscatters* the components of the incident polarization state. For a randomly oriented ensemble

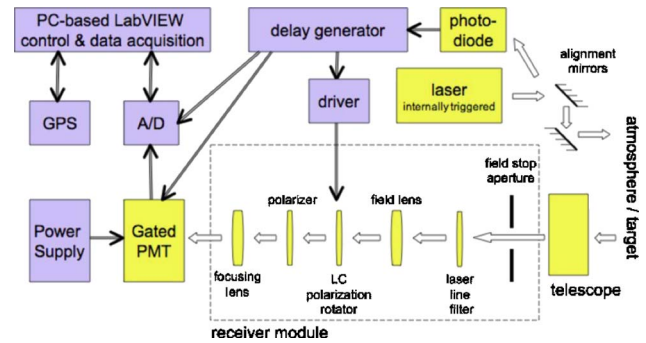


Fig. 1 Schematic of the Montana State University dual-polarization lidar system.

of crystals, we should expect a significant cross-polarized component in addition to a co-polarized component. So there is a clear mechanism for backscatter depolarization of single-scattered light from ice crystals. For spherical water droplets, there is no mechanism for depolarization apart from multiple scattering effects.

A depolarization ratio of 1 is the theoretical limit for randomly oriented particles. Sassen¹⁴ measured $\delta=0.03$ for liquid water droplets and $\delta=0.5$ for ice crystals in laboratory experiments. The values often accepted for cloud depolarization are $\delta < 0.03$ for water and $\delta=0.4$ to 0.5 for ice, although the value for ice can vary over approximately 0.2 to 0.8 .¹ Although there is significant geographic variability, $\delta \leq 0.25$ is one criterion that has been used to identify liquid-dominated mixed-phase clouds in midlatitude Rocky Mountain clouds.¹⁵ (The data we show were all collected at Bozeman, Montana, in the Rocky Mountains at 45.67°N , 111.05°W). Depolarization ratios larger than 0.7 are characteristic of snowflakes, because of their more complex shape. Variation of depolarization from different crystals is a result of the relative importance of normal-incidence back-reflections off outside surfaces, as opposed to reflections off inner surfaces, which involve oblique angles. For example, it is possible to measure zero depolarization when the laser is pointed to provide normally incident specular reflection from horizontal ice crystals.^{1,16}

3 Instrument Description

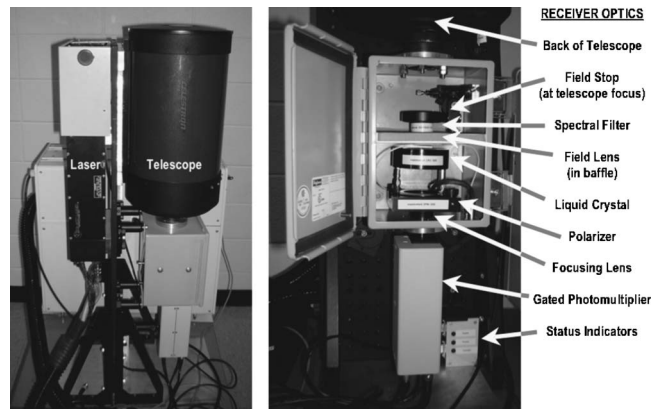
The lidar system is composed of a laser transmitter, a receiver telescope, receiver and detector optics, a signal digitizer, timing and power supply electronics, and a computer for control and data recording. Figure 1 shows a schematic of the relations between these parts. The 532-nm laser pulses are triggered internally by the laser power supply at 30 Hz. A photodiode near the laser detects the pulses and triggers a delay generator, which controls the timing of the rest of the system. The transmitter beam is directed out of the lidar with two steering mirrors (Newport mirrors, coated for high-power green light at 532 nm and for operation at 45-deg incidence). Shot-to-shot energy variations are less than 2%, and with temporal averaging and median filtering (described in Sec. 5), the effect of this is reduced to insignificant levels well below 1%.

The receiver telescope is a Schmidt-Cassegrain system with a 20.3-cm-diam primary aperture and a 6.9-cm-diam secondary mirror obscuring the center of the aperture, pro-

Table 1 Summary of system specifications.

| Transmitter: Big Sky Laser CFR200, Flashlamp-Pumped Frequency-Doubled Nd:YAG | |
|--|---|
| Wavelength | 532 nm |
| Pulse repetition rate | 30 Hz |
| Pulse energy | 118 mJ |
| Beam divergence | 2.16 mrad |
| Pulse width | 10 ns |
| Receiver: Celestron 8" Schmidt-Cassegrain Telescope | |
| Focal length | 2265 mm |
| Field of view | Variable up to 8.8 mrad |
| Spectral filter | 1-nm FWHM |
| Detector | Hamamatsu Gated PMT |
| Signal Processing: Gage 14100, PCI-Based Digitizer | |
| Sample rate | 100 MS/s (1.5-m sampling period) |
| Nominal bit depth | 14 bits |
| Data rate | 2.16 GB/hour (with 15-km range and full resolution) |
| Polarization Discrimination: Meadowlark Optics Nematic Liquid Crystal Variable Retarder | |
| System depolarization ratio additive error | <0.4% |
| Instrument Size (W×L×H) | |
| Optics package | 31 cm×46 cm×97 cm |
| Electronics rack | 59 cm×89 cm×87 cm |

viding an effective aperture area of 286.3 cm². The telescope directs received light through a field stop, interference filter (1-nm bandwidth centered at 532 nm), field lens, and polarizing optics, all contained in a light-tight box. The field-stop size can be changed to vary the receiver field of view up to 8.8 mrad. The interference filter is placed in the optical space with the shallowest ray angles (<2.8 deg at the 8.8-mrad maximum field of view) to minimize angular tuning of the filter bandwidth. (The field lens redirects off-axis rays back toward the detector, but does so at steeper angles.) At the output of the optics box is a gated photomultiplier tube (PMT) detector whose output current is sampled [as a voltage across the analog-to-digital (A/D) card 50 Ω impedance] by a fast and high-resolution A/D converter that resides in the computer. The 10-ns laser pulse duration and the A/D sample rate of 100 MS/s both limit the range resolution to 1.5 m. Table 1 is a summary of

**Fig. 2** Photographs of the lidar optics package (left) and detail of the receiver optics (right).

system specifications, and Fig. 2 shows two photographs of the system. The optics package is relatively compact, consisting of a 30.5 cm×91.5 cm aluminum plate, mounted vertically on a base, with the transmitter on one side and the receiver on the other.

At the widest field-of-view setting, the transmitter and receiver beams are in full overlap at altitudes between 80 m and beyond 15 km, where we end data acquisition. (The minimum range for data acquisition is 10 m, determined by delays in the electronics.) For the current biaxial configuration with a raw, unexpanded laser beam, the minimum overlap altitude moves upward at narrower receiver fields of view. Overlap calculations⁷ show that the minimum altitude for 99.9% overlap is 80 m at 8.8-mrad field of view and rises to 500 m at 4.4 mrad. 90% overlap is achieved at 450 m with a 2.6-mrad field of view. A very small field of view (≤ 1 mrad), which is necessary to minimize the effects of multiple scattering in thick clouds, will be made more practical in this system with future modifications that include expansion of the transmitted laser beam.

The most unique feature of the system is the method of discriminating between polarization states with a liquid crystal and polarizer. Many lidar systems use a polarizing beamsplitter and two detectors,¹⁷ and some use multiple telescopes.³ Either way, this requires calibrating for the difference between the detectors. Another method is to measure only one polarization at a time, but to alternate the sampled polarization quickly enough that the target is presumed not to have changed. The depolarization ratio is computed between different pulses, or between different sets of pulses. This approach provides advantages of smaller size and fewer components. It is also simpler to calibrate a system with one detector. The disadvantage is a loss of time resolution (because there are fewer useful pulses—not a loss of sampling resolution for a given pulse). The alternating-pulse method has been implemented in NOAA's Depolarization And Backscatter Unattended Lidar (DABUL) using a Pockels cell.¹⁸ Pockels cells generally have small apertures and long lengths, which can be a difficulty for wide fields of view.

We tested a ferroelectric liquid crystal, which has only two stable orientations for the molecules, so it provides switching between only two retardance values. These de-

vices are thinner and faster than other liquid crystals, but since the retardance was not exactly right and it was not tunable with voltage, the measured depolarization ratio error was worse than 3%.

We built our lidar with a nematic liquid crystal, which provides retardance that is tunable with an applied voltage. With a compensating waveplate integrated by the manufacturer, the retardance can be tuned down to zero (and slightly below). We use a Meadowlark Optics temperature-controlled nematic liquid crystal variable retarder, with a 4-cm clear aperture. The slow axis of the device is oriented at 45 deg to the transmitted polarization. It is switched between zero and $\lambda/2$ retardance, and followed by a Meadowlark film polarizer (better than $10^5:1$) oriented parallel to the transmitted polarization. The zero-retardance state measures co-pol light and the $\lambda/2$ -retardance state measures cross-pol light by rotating it to be passed by the polarizer. To our knowledge, the only other instance of a liquid crystal being used to provide lidar polarization switching is a dual-polarization version¹⁹ of the Micro Pulse Lidar (MPL)²⁰ system being developed at the Pacific Northwest National Laboratory for the Department of Energy Atmospheric Radiation Measurement (ARM) Program, using the same model liquid crystal device.

The liquid crystal switching speed was a concern because we switch in the time between consecutive laser shots (at 30 Hz). The switching speed is quicker at higher temperatures and at higher voltages. It is also quicker for the transition to a higher voltage (to less retardance) because the opposite transition relies on the relaxation to the natural state of the crystal. A common strategy is to overshoot the desired voltage for a short time to speed up the transition, called the Transient Nematic Effect.²¹ We operate the device at 40°C, and at this temperature for this device, the voltages for $\lambda/2$ and zero retardances at 532 nm are found to be 2.055 V and 4.950 V, respectively. The wave form supplied by the driver is a 2-kHz square wave, centered on 0 VDC to keep charge from building up on the liquid crystal. The amplitude envelope of this square wave is switched between ± 2.055 and ± 4.950 V during the time period between 30-Hz laser pulses. The waveform envelope is programmed to switch between 2.055 V and 4.950 V, but the first 5 ms for each transition are overshoot to 10 V and 0 V. The resulting switching times are 22 ms to go from zero to $\lambda/2$ retardance and 9 ms to go from $\lambda/2$ to zero retardance. This is fast enough to allow switching between 30-Hz laser pulses (33-ms period) if the device is switched soon after the laser pulse. Although this is significantly slower than the switching speeds of Pockels cells, the liquid crystal uses much lower voltages that do not produce noticeable switching noise.

Both the retardance and effective angle of rotation of a liquid crystal depend on incidence angle. For the widest field of view, the ray angle in this region of the receiver is less than 5 deg. Xiao et al.²² showed that for similar conditions (a liquid crystal oriented at 45 deg and set near a $\lambda/2$ retardance), external incidence angles of 5 deg cause the retardance to vary by about 0.08λ and the 45 deg rotation angle to vary by about 2 deg. With both of these errors at their worst, the resulting Mueller matrix predicts that the cross-polarized signal (with no target depolarization) is 2.0%. However, only a small fraction of the light is

likely to have a 5 deg incidence angle. Predicting this is not as simple as integrating over all accepted incidence angles, since this would ignore the location of the beam within the field, which varies with range (and depends on the laser-telescope inclination angle, the divergence of the laser, the telescope field of view, and the horizontal separation between the laser and telescope). No measurement will have a full 2% error from this source, but this provides another reason to prefer narrower fields of view (smaller ray incidence angles). The data presented in Sec. 6 were all taken with the maximum field of view (8.8 mrad), which helps confirm that the LCVR technique works well at this setting. The LCVR technique will work even better at smaller fields of view that are needed to reduce multiple scattering in cloud lidar signals.

4 Instrument Polarization Characterization

To find the accuracy of the lidar depolarization measurements, the laser, the telescope, and the liquid crystal are the most crucial elements to characterize polarimetrically. The following description of the system will fall short of a full Stokes parameterization; light that is incident on the receiver is treated as being composed exclusively of linear co-pol and linear cross-pol components.

A 5-mW CW, 532-nm Nd:YAG laser source was used for the tests, with a Glan-laser polarizer specified with $10^5:1$ extinction. The polarization of this beam was assumed to be perfectly linear. Using this ideal reference beam, a film polarizer used as an analyzer (specified at an extinction of $10^4:1$) was found to be better than $7 \times 10^4:1$. These values impose limits on the measurements of the system components.

4.1 The Laser Transmitter

Good receiver polarization discrimination is useless without a highly polarized transmitter. The pulsed-laser polarization was measured with the Glan-laser polarizer and a volume-absorbing calorimeter (without filters). With transmitted average powers of 3.2 W with the polarizer aligned vertically and 2.4 mW with the polarizer aligned horizontally, the laser was determined to be linear to 7.5×10^{-4} (1,333:1). The two beam-steering mirrors in the system are designed for high energies at 532 nm with 45-deg incidence angle. These mirrors have a higher reflection, but slightly worse depolarization, compared to standard uncoated mirrors. The mirrors are oriented such that the polarization of the incident light is perpendicular to the plane of reflection (the *S* polarization). Measurements of both coated and uncoated mirrors show that the reflection is better for incident *S* polarization, and the polarization is better maintained for incident *P* polarization. However, the depolarization of the mirrors in this configuration is still good to $2.9 \times 10^4:1$, so this is not an issue.

4.2 The Telescope

The telescope could potentially depolarize the beam with its optical coatings and oblique mirror reflections. Testing the telescope is a bit tricky since it is hard to come by a linearly polarized beam of collimated light that fills the 20-cm aperture. We tested the telescope three ways:

Table 2 Measured transmissions of the assembled receiver (with the liquid crystal set for zero and half-wave retardances) for different incident linear polarization states. Measured with a laser-line interference filter with $T=0.5212$.

| | | Liquid Crystal Setting | | |
|--------------------------|------------------------|--------------------------------------|--|--|
| | | Zero retardance (4.950 V on LCVR) | Half-wave retardance (2.055 V) on LCVR | Liquid crystal removed from system |
| Incident polarization | <i>Co-polarized</i> | $T_{0\parallel}=0.3653$ | $T_{\lambda/2\parallel}=0.0014$ | $T_{\parallel}=0.3993$ |
| | <i>Cross-polarized</i> | $T_{0\perp}=0.0019$ | $T_{\lambda/2\perp}=0.3651$ | $T_{\perp}=2.0 \times 10^{-4}$ |

- 1 With a laser beam diverged to fill the aperture, but not collimated
- 2 With a narrow laser beam aimed at different places on the primary mirror with normal ray angles, but without filling the aperture
- 3 With skylight passed through a large sheet polarizer, which both fills the aperture and is collimated, but has less-certain polarization.

For the first method (with no field stop at the telescope focus), the ray incidence angles were not realistic since the beam was diverging severely. Because the source was in the near-field of the telescope, the beam exiting the telescope was doughnut-shaped owing to the central obstruction. By varying the position of the source within the field of view, the measured depolarization of the exiting beam varied from 1.12×10^{-4} to 3.53×10^{-4} (8,929:1 to 2,833:1).

In the second method (again with no field stop at the telescope focus), the narrow laser beam was aimed at eight different points on the primary mirror, some near the center and some near the edge. All points yielded depolarization better than 3.06×10^{-5} (32,680:1). Some were as good as 1.50×10^{-5} (66,667:1), whereas, with the telescope entirely removed, the beam depolarization was 1.17×10^{-5} (85,470:1). There was no clear correlation between the beam position on the primary mirror and the depolarization, but the beam position on the secondary mirror was undetermined and this could possibly have an effect.

The third method, aiming the telescope at the daytime sky with a sheet polarizer covering the telescope aperture (with the field stop in place behind the telescope), is attractive because it fills the telescope aperture with light from far away. The disadvantage is that measurements had to be taken quickly so that the polarization and irradiance of the skylight could be assumed not to have changed. (This is better on a completely clear day than on a completely overcast day.) A large sheet polarizer (rated at 100:1) was used, covering the front of the telescope, to make the skylight as linearly polarized as possible. (To reduce the effect of variable skylight polarization, the telescope was pointed near the region of minimal Rayleigh scattering polarization.) The light from the telescope was passed through a laser line filter and an analyzing polarizer and focused onto a detector. In two measurements, the depolarization of the light exiting the telescope was 5.49×10^{-4} and 5.10×10^{-4} (1,821:1 and 1,961:1). With a second sheet polarizer added

in front of the telescope, with its polarization axis coaligned with the first, the polarization purity of the exiting beam improved to 4.68×10^{-4} (2,137:1). The skylight measurements, being well below the quality of the polarizers, are used only to give an upper limit to the telescope depolarization. None of the three methods found telescope depolarization to be very large, probably owing to the small incidence angles involved.

4.3 The Liquid Crystal and the Assembled Receiver

Rather than testing the liquid crystal and polarizer individually, we tested the whole assembled lidar receiver because this could reveal misalignments between the components. Tests of individual components tell whether or they are good enough to be a part of the system, but this test will show the accuracy of the lidar depolarization measurements.

In this case, the test is of how well the desired incident polarization is selected—the analyzer is built into the device under test (the LCVR-polarizer combination in its co-pol and cross-pol settings). The lidar was aimed horizontally on an optics table and both co-pol (vertical) and cross-pol (horizontal) light were made incident, one at a time. It is crucial to align the polarization of the input beam precisely, so the part of the beam rejected out across the room by the Glan-laser polarizer was used as an indicator of the polarizer's orientation. For each input polarization, the power was measured before the telescope and again behind the receiver optics box and the transmission calculated. This measurement was done four times—once for each combination of input polarization and liquid crystal state (Table 2). We emphasize that the transmittances in Table 2 are measurements for the entire optical receiver, made with an ideal linearly polarized input source. (They are not transmittances of only one optical element.) Also, various other configurations, such as with the liquid crystal removed, were tested.

These transmission measurements are useful both for finding the error in lidar depolarization ratios and for calibrating the system radiometrically. Note that $T_{\lambda/2\perp}$ and $T_{0\parallel}$ are the transmissions of the two polarization states when you intend to measure each of those states by setting the liquid crystal appropriately. It is good that these transmis-

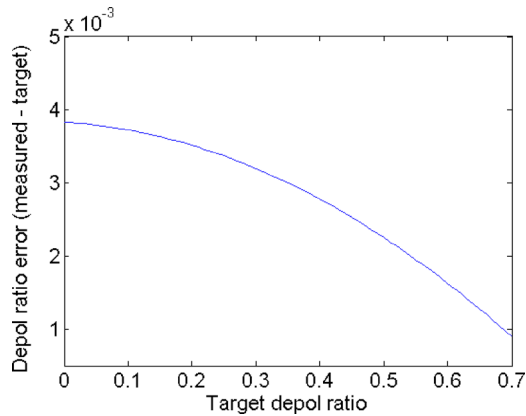


Fig. 3 Additive error in the measured lidar depolarization ratio (for the whole assembled receiver) as a function of the target depolarization ratio.

sions are the same, and achieving this requires very precise alignment. On the other hand, $T_{\lambda/2\perp}$ and $T_{0\perp}$ are the ones that should be minimized.

To find the error in depolarization ratios, first recall that the depolarization caused by a target scattering object is the ratio of the two linearly polarized optical powers *incident on the receiver*, $\delta_{target} = P_{\perp} / P_{\parallel}$. However, the measured depolarization ratio is the ratio between the signals *incident on the detector* for the two liquid crystal states:

$$\delta_{measured} = \frac{T_{\lambda/2\perp} P_{\perp} + T_{\lambda/2\parallel} P_{\parallel}}{T_{0\perp} P_{\perp} + T_{0\parallel} P_{\parallel}}. \quad (2)$$

This can be neatly rewritten in terms of the target depolarization:

$$\delta_{measured} = \frac{T_{\lambda/2\perp} \left(\frac{P_{\perp}}{P_{\parallel}} \right) + T_{\lambda/2\parallel}}{T_{0\perp} \left(\frac{P_{\perp}}{P_{\parallel}} \right) + T_{0\parallel}} = \frac{T_{\lambda/2\perp} \delta_{target} + T_{\lambda/2\parallel}}{T_{0\perp} \delta_{target} + T_{0\parallel}}. \quad (3)$$

The additive error in a measured depolarization ratio is $\Delta\delta = \delta_{measured} - \delta_{target}$. Using the transmissions from Table 2, the error is plotted in Fig. 3 for target depolarization ratios of 0 to 0.7. The worst case is an additive error of 0.0038, about 0.4%. This is an acceptable error for depolarization ratio measurements, which often are not stated to better than 1%. The worst error occurs when δ_{target} is zero. This is easily explained as follows: If the system has a depolarization such that it mixes a fixed fraction of the co-pol and cross-pol signals into the other, the net effect will be less when the two signals are comparable to begin with. It is worth noting that the ratio $T_{\lambda/2\perp} / T_{0\parallel}$, the receiver transmittances measured with the LCVR retardance set to $\lambda/2$ and 0, respectively, while the receiver is illuminated with co-polarized light, gives the 0.0038 worst-case depolarization error mentioned earlier. A similar ratio of transmittances measured with cross-polarized incident light ($T_{0\perp} / T_{\lambda/2\perp}$) gives 0.0052, but this ratio describes a case where the receiver is illuminated with purely cross-

polarized light. (This situation is not relevant, since we define 100% depolarization as the presence of equal amounts of co-polarized and cross-polarized light.)

5 Sample Data

The lidar data acquisition software saves a data file for each minute of operation. Since there are 10,112 samples per laser shot, 1,800 shots per minute (at 30 Hz), and 88 rows of footer data, the file format is an array $10,200 \times 1,800$. (The status of the liquid crystal, determining whether it is a co-pol or cross-pol shot, and other system settings are stored in this array as a footer.)

In processing the data, the co-pol and cross-pol shots are compiled into separate arrays. A shot-to-shot, three-point median filter is run across the whole minute-long data file, which allows single-pixel extreme values to be filtered out. Occasionally, a shot appears as if the liquid crystal failed to switch (a column in the array with values unlike those on each side). The purpose of a horizontal median filter is to remove this, as well as random noise.

Next we remove background sky noise, which is constant in the sampling dimension but which varies significantly with time, especially during the daytime. The varying sky noise is very small and may not be obvious in the co-pol signal, but the depolarization ratio is highly dependent on small cross-pol values. To get the ratio correct, different sky background levels must be subtracted from the co-pol and cross-pol signals first. (The skylight is partially polarized, so the background levels change depending on the polarization state of the receiver). The offset is computed for each shot by taking the median of the samples in the range of 14 to 15 km, with the assumption that there is no signal at this range. If there are no aerosols present at this range, this signal-correction procedure effectively removes the molecular depolarization signal. (Alternative schemes could be used to calibrate the two polarization channels in a way that would retain the molecular signal.²³) The offset-corrected data are range corrected by multiplying by the range (in km) squared, removing the explicit $1/r^2$ dependence of the signal.²⁴ Finally, a depolarization ratio array is computed by dividing the cross-pol data array by the co-pol array, element by element. When the signals fall into the noise, the displayed depolarization randomly varies between the extremes.

The observed depolarization ratio can be affected by multiple scattering in clouds at a wide field of view. For example, multiple scattering causes the depolarization ratio to steadily increase as the beam penetrates into the bottom of a thick water cloud. We have taken data at a variety of fields of view and have observed multiple scattering effects in thick clouds at the wider settings. The data we show here happen to have been taken with a wide 8.8-mrad field-of-view setting, but we show only data for thin scattering layers that do not exhibit any obvious increase of depolarization with penetration depth in the cloud. One important motivation for taking wide-field data is to evaluate the LCVR-polarization-switching technique with the wide field of view that will be particularly useful in marine, biological, terrestrial, and vegetation applications.³⁻⁶

If the lidar is used for quantitative retrievals of cloud optical properties, a much narrower field of view is required. The actual impact of multiply scattered light on

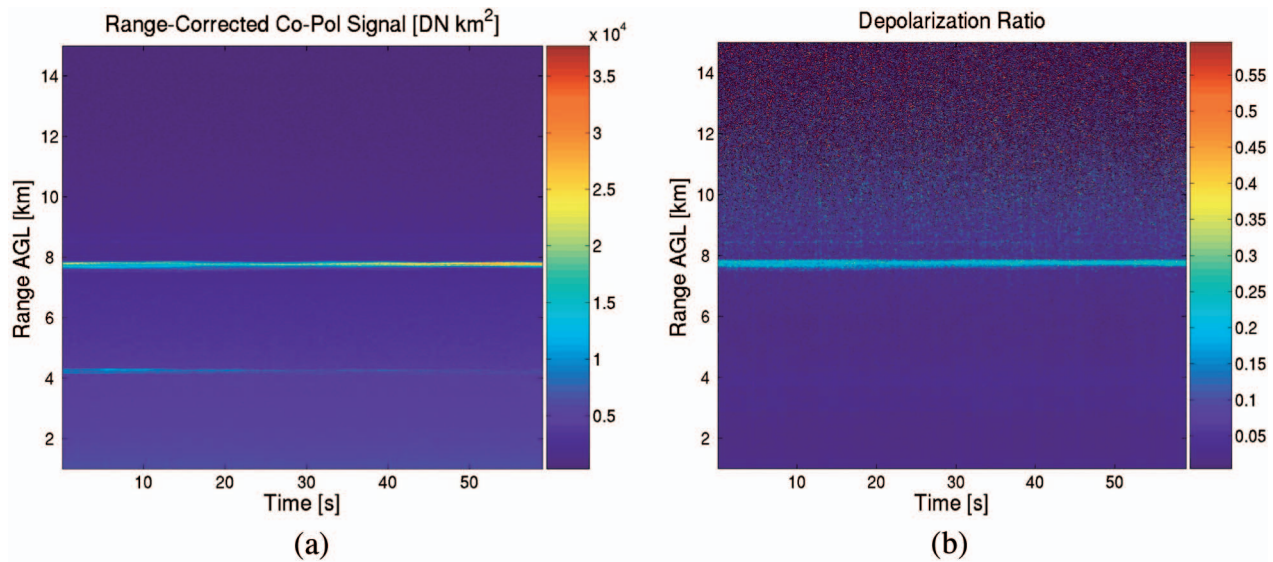


Fig. 4 Lidar data time-height plot for 3 March 2005, 04:19 UTC, showing multiple cloud or aerosol layers with different depolarizations. (a) Range-corrected co-pol signal; (b) depolarization ratio.

lidar data depends in a very complex manner on range, optical depth, transmitter divergence, and receiver field of view.^{25–28} While multiple scattering seems to be a second-order effect that can be safely neglected in measurements of aerosol scattering (except in extremely hazy conditions such as dust storms and extreme pollution events),²⁹ multiple scattering contributes significantly to cloud lidar signals, especially for optically thick clouds. A variety of studies indicate that for ground-based lidars with a full-angle receiver field of view comparable to or smaller than approximately 1 mrad, multiple scattering effects contribute errors smaller than other uncertainties typically present in retrievals of optical properties from lidar data.^{25–28} However, because the extremely long ranges cause even small

angular fields to enclose large cloud volumes, multiple scattering cannot be neglected even with small fields of view in space-based lidars.²⁸ Recently there has been significant effort made to exploit multiple scattering for enhanced lidar retrievals.³⁰

Figures 4–7 show sample data that illustrate the water-phase discrimination capabilities of the dual-polarization lidar. We show time-height plots, which are useful for evaluating the temporal evolution of the signal and the temporal stability of the instrument, and vertical profiles, which are useful for evaluating the vertical distribution of scattering and depolarization at a fixed time. The vertical air-

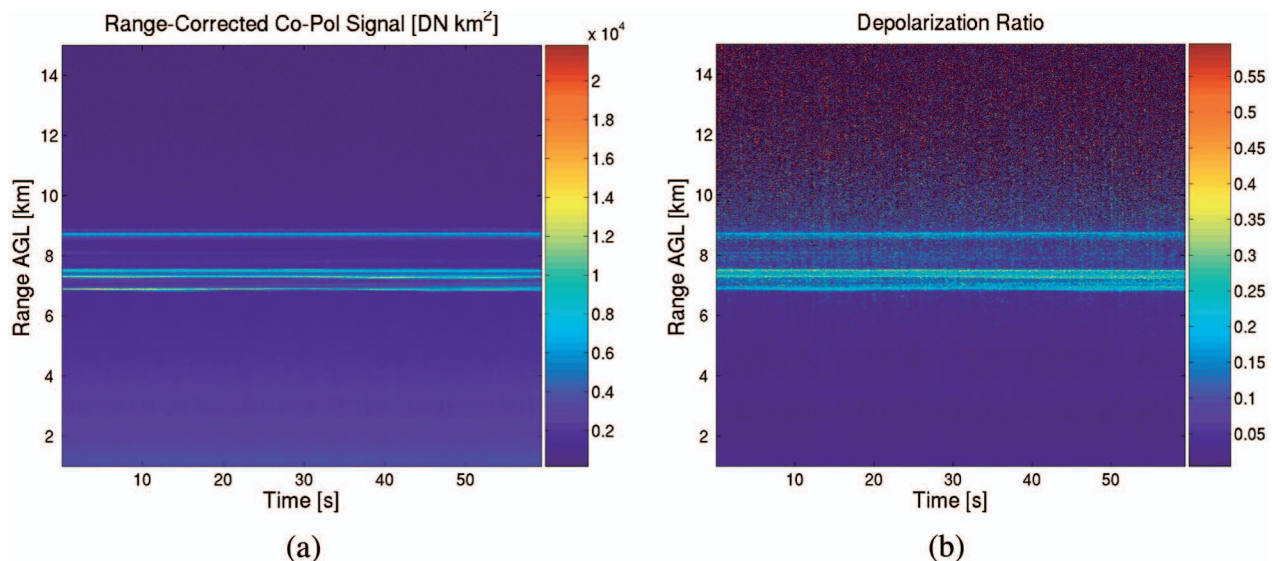


Fig. 6 Lidar data time-height plot for 1 March 2005, 03:32 UTC, showing multiple subvisual layers of depolarizing material. (a) Range-corrected co-pol signal; (b) depolarization ratio.

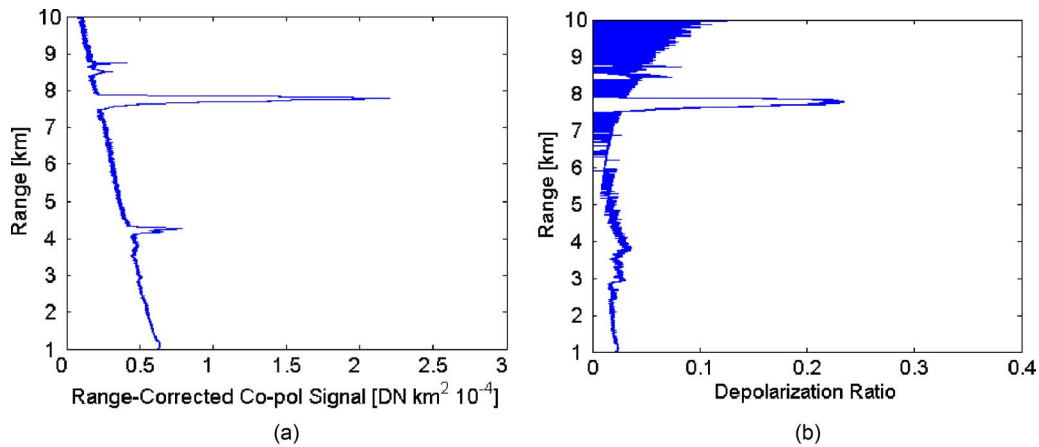


Fig. 5 Vertical profiles for 3 March 2005, 04:19 UTC, 10 s into the time-height plot of Fig. 4. (a) Range-corrected co-pol signal; (b) depolarization ratio.

temperature (T) profile data referred to in the following discussion were obtained from radiosondes launched on balloons during the lidar data acquisition.

Figures 4 and 5 (3 March 2005, 04:19 UTC) show two narrow layers with very different depolarization ratios. Figure 4 is a time-height plot that initially shows two thin layers, but the lower layer disappears by the middle of the plot. Figure 5 shows height profiles, taken approximately 10 s into Fig. 4, of (a) the co-polarized backscatter signal and (b) the depolarization ratio δ . The lower layer, at an altitude of 4.2 km ($T=-25^{\circ}\text{C}$), has $\delta=0.023$, which is typical for super-cooled liquid clouds. Above this liquid layer is another thin layer at 7.8 km, with temperature well below -40°C . (The radiosonde launch terminated early.) This higher layer is probably ice but could also be an aerosol layer (see discussion of Figs. 6 and 7). Two additional layers can be seen at 8.4 and 8.6 km, both with depolarization ~ 0.1 . These are so faint (~ 25 DN), that the depolarization ratio value is questionable. These layers could be either subvisual cirrus or elevated aerosol layers.

Measurements of a similar set of elevated scattering layers two days earlier are shown in Figs. 6 and 7 (1 March

2005, 03:32 UTC). These figures show at least four distinguishable depolarizing layers between 6.9 and 8.7 km. All these layers were subvisual, with stars clearly visible through them. The temperature at these altitudes ranged from -47 to -60°C , and δ ranged from 0.18 to 0.25. The temperature and depolarization ratio suggest that these layers are either subvisual cirrus (ice) or aerosols, or some combination thereof. Our radiosonde data show the relative humidity over ice to be less than 40% below 8 km and near 100% between 8 and 9 km. Therefore, the depolarizing layers above 8 km could be subvisual cirrus, but this does not necessarily explain the layers at lower altitudes (~ 7 to 8 km). An alternative explanation for at least some of the high, thin, depolarizing layers observed consistently over the period 1 to 3 March is elevated aerosol layers or a combination of aerosols and thin cirrus clouds nucleated by the dust.³¹

It is known that dust or pollution from Asia can be blown across the Pacific and appear as elevated depolarizing layers over the United States. Asian dust has been observed by lidars in Japan, Alaska, Utah, and Colorado, to name a few, primarily during the spring season.³² Dust has

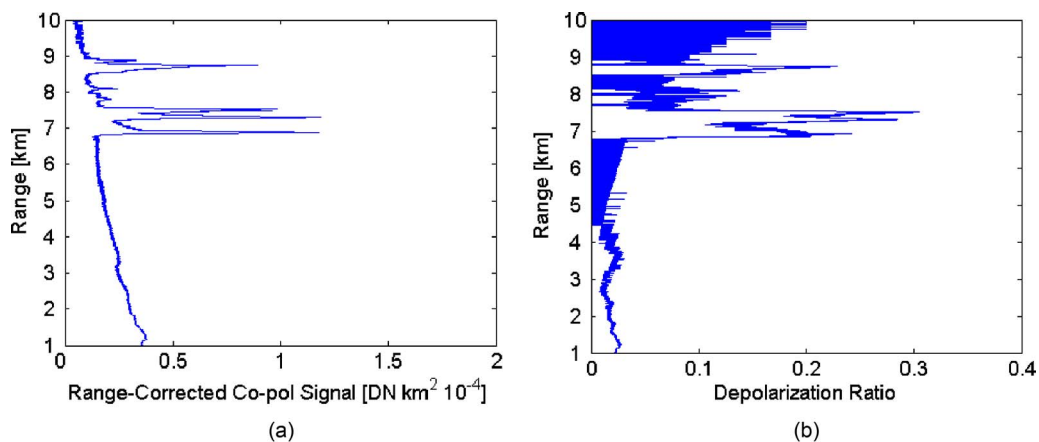


Fig. 7 Vertical profiles for 1 March 2005, 03:32 UTC. (a) Range-corrected co-pol signal; (b) depolarization ratio.

been observed with depolarization ratios up to ~ 0.25 ,^{17,31,33} and since the presence of dust can cause cirrus ice particles to nucleate, it has also been observed mixed with cirrus.³¹ A back-trajectory analysis of the atmosphere at different altitudes over Bozeman was performed with the NOAA HYSPLIT model,³⁴ using defaults for the vertical transport model. This analysis shows that air from 7500-m above ground level over Bozeman came from 3500 m over east-central China ten days earlier. The probability is low that the air mass was loaded with dust or other depolarizing aerosols in an intermediate location because, before entering Montana, the trajectory spent less than three days over western Canada during a period devoid of forest fires and characterized by very low convective available potential energy (CAPE) in radiosonde profiles from the region, and prior to that it was over open ocean since leaving the China coast near the start of the ten-day period.

Around 20 February 2005, there was thick haze over Beijing and most of central China, but the air was very stable, so the likelihood is low that haze could have risen out of the boundary layer to an altitude where it would be blown eastward. It is more likely that sand on the Tibetan plateau, at an elevation of about 3500 m, was blown across this stable air and out over the Pacific.^{35,36} (Rawinsonde data indicate strong westerly winds over the Tibetan plateau and across central China during this time period.) Given all the available information, Asian dust mixed with subvisual cirrus appears to be a reasonable explanation of these observations.

6 Discussion and Conclusions

We have built and characterized a dual-polarization lidar that uses a liquid crystal variable retarder (LCVR) to switch the receiver polarization state on alternate laser shots, determining a target depolarization ratio 15 times per second (for a 30-Hz laser pulse repetition frequency). This allows the use of a single detector, eliminating the need for calibrating separate detectors, and potentially reducing size, cost, and weight. The system characterization required determining the response of the instrument to two orthogonal polarization states of light. The characterization measurements (summarized in Table 2) show that the end-to-end polarization sensitivity is within 0.4%. In fact, 0.4% is the maximum additive depolarization ratio error, the worst case, which occurs when the target depolarization is zero. Sample data demonstrate the effectiveness of the system to discriminate between liquid or ice in clouds. We also observed a thin scattering layer near an 8-km altitude that appears to be subvisual cirrus, aerosols that originated in Asian dust storms, or possibly a combination of these two.

Temperature stabilization and careful treatment of the receiver field of view were both necessary for successful incorporation of an LCVR for polarization switching. This particular lidar has a variable field of view, which at the upper end can allow multiple scattering in clouds to become significant. The presented data show only thin layers, which exhibit none of the characteristics of multiple scattering (increase in depolarization ratio from 0 to 0.4 over about 150 to 200 m of cloud penetration). We also have obtained data, not shown here, for thicker clouds that do show exactly this behavior. Consequently, future modifications will include expanding the transmitter beam to im-

prove overlap when the receiver is used with a narrow field of view. The LCVR-based receiver works well over the entire field-of-view range, but use of a narrow field of view is preferable because of angle-dependent variations of LCVR retardance.

LCVR switching can just keep up with a 30-Hz laser pulse repetition frequency, but if this technique were to be used in a micropulse lidar or other lidar with faster pulse rate, the polarization receiver state could be switched between blocks of pulses at each state. The liquid crystal switching adds no noticeable noise to the data acquisition system. Overall, the LCVR polarization switching technique is useful for electronically switching between polarization states, which provides some simplification and size reduction relative to lidars with separate polarization channels.

Acknowledgments

The lidar was developed with funding from the NASA Ames Research Center, and Nathan Seldomridge was supported on a NASA Graduate Student Researchers Program (GSRP) fellowship sponsored by Dr. Bruce Davis at the Stennis Space Center. The authors gratefully acknowledge the NOAA Air Resources Laboratory (ARL) for the provision of the HYSPLIT transport and dispersion model used in this publication.

References

1. K. Sassen, "The polarization lidar technique for cloud research: a review and current assessment," *Bull. Am. Meteorol. Soc.* **72**, 1848–1866 (1991).
2. J. A. Reagan, M. P. McCormick, and J. D. Spinhirne, "Lidar sensing of aerosols and clouds in the troposphere and stratosphere," *Proc. IEEE* **77**, 433–448 (1989).
3. S. Tan and R. N. Narayanan, "Design and performance of a multi-wavelength airborne polarimetric lidar for vegetation remote sensing," *Appl. Opt.* **43**, 2360–2368 (2004).
4. J. E. Kalshoven Jr. and P. W. Dabney, "Remote sensing of the Earth's surface with an airborne polarized laser," *IEEE Trans. Geosci. Remote Sens.* **31**, 438–446 (1993).
5. J. H. Churnside, J. W. Wilson, and V. V. Tatarskii, "Airborne lidar for fisheries applications," *Opt. Eng.* **40**, 406–414 (2001).
6. J. A. Shaw, N. L. Seldomridge, D. L. Dunkle, P. W. Nugent, L. H. Spangler, J. J. Bromenshenk, C. B. Henderson, J. H. Churnside, and J. W. Wilson, "Polarization lidar measurements of honey bees for locating land mines," *Opt. Express* **13**, 5853–5863 (2005).
7. N. L. Seldomridge, "Dual-polarization cloud lidar design and characterization," MS Thesis, Electrical and Computer Engineering Department, Montana State University, Bozeman, MT, available online at: www.montana.edu/etd/available/seldomridge_0805.html (2005).
8. K. N. Liou, *An Introduction to Atmospheric Radiation*, 2nd ed., International Geophysical Series, Vol. **84**, Academic Press, San Diego, CA (2002).
9. K. N. Liou, "Influence of cirrus clouds on weather and climate processes: a global perspective," *Mon. Weather Rev.* **114**, 1167–1199 (1986).
10. A. J. Heymsfield and C. M. R. Platt, "A parameterization of the particle size spectrum of ice clouds in terms of the ambient temperature and the ice water content," *J. Atmos. Sci.* **41**, 846–855 (1984).
11. S. Twomey, "Pollution and the planetary albedo," *Atmos. Environ.* **8**, 1251–1256 (1974).
12. R. M. Schotland, K. Sassen, and R. Stone, "Observations by lidar of linear depolarization ratios for hydrometeors," *J. Appl. Meteorol.* **10**, 1011–1017 (1971).
13. K. N. Liou and H. Lahore, "Laser sensing of cloud composition: a backscattered depolarization technique," *J. Appl. Meteorol.* **13**, 257–263 (1974).
14. K. Sassen, "Depolarization of laser light backscattered by artificial clouds," *J. Appl. Meteorol.* **13**, 923–933 (1974).
15. K. Sassen and H. Zhao, "Supercooled liquid water clouds in Utah winter mountain storms: cloud-seeding implications of a remote-sensing dataset," *J. Appl. Meteorol.* **32**, 1548–1558 (1993).
16. C. M. R. Platt, N. L. Abshire, and G. T. McNice, "Some microphysical properties of an ice cloud from lidar observation of horizontally

- oriented crystals," *J. Appl. Meteorol.* **17**, 1220–1224 (1978).
17. N. Sugimoto, I. Matsui, A. Shimizu, I. Uno, K. Asai, T. Endoh, and T. Nakajima, "Observation of dust and anthropogenic aerosol plumes in the Northwest Pacific with a two-wavelength polarization lidar on board the research vessel Mirai," *Geophys. Res. Lett.* **29**, doi: 10.1029/2002GL015112(2002).
 18. J. M. Intrieri, M. D. Shupe, T. Uttal, and B. J. McCarty, "An annual cycle of arctic cloud characteristics observed by radar and lidar at SHEBA," *J. Geophys. Res.* **107**, doi: 10.1029/2001JC000423(2002).
 19. C. J. Flynn, MS K9-24, Battelle NW, Pacific Northwest National Laboratory, Richland, WA, Private Communication (2005).
 20. J. R. Campbell, D. L. Hlavka, E. J. Welton, C. J. Flynn, D. D. Turner, J. D. Spinhirne, V. S. Scott III, and I. H. Hwang, "Full-time, eye-safe cloud and aerosol lidar observation at atmospheric radiation measurement program sites: instruments and data processing," *J. Atmos. Ocean. Technol.* **19**, 431–442 (2002).
 21. *Response Time in Liquid-Crystal Variable Retarders*, Application Note, Meadowlark Optics (2003), <http://www.meadowlarkoptics.com/applicationNotes>
 22. X. Xiao, D. Voelz, and H. Sugiura, "Field of view characteristics of a liquid crystal variable retarder," in *Proc. SPIE* **5158**, 142–150 (2003).
 23. A. Behrendt and T. Nakamura, "Calculation of the calibration constant of polarization lidar and its dependency on atmospheric temperature," *Opt. Express* **10**(16), 805–817 (2002).
 24. R. M. Measures, *Laser Remote Sensing*, p. 243, Wiley and Sons, New York (1984).
 25. K. E. Kunkel and J. A. Weiman, "Monte Carlo analysis of multiply scattered lidar returns," *J. Atmos. Sci.* **33**, 1772–1781 (1977).
 26. C. M. R. Platt, "Remote sounding of high clouds. III: Monte Carlo calculations of multiple-scattered lidar returns," *J. Atmos. Sci.* **38**, 156–167 (1981).
 27. K. Sassen and R. L. Petrilla, "Lidar depolarization from multiple scattering in marine stratus clouds," *Appl. Opt.* **25**, 1450–1459 (1986).
 28. D. M. Winker and L. R. Poole, "Monte-Carlo calculations of cloud returns for ground-based and space-based lidars," *Appl. Phys. B* **60**, 341–344 (1995).
 29. J. Ackermann, P. Völger, and M. Wiegner, "Significance of multiple scattering from tropospheric aerosols for ground-based backscatter lidar measurements," *Appl. Opt.* **38**, 5195–5201 (1999).
 30. L. R. Bissonnette, G. Roy, and N. Roy, "Multiple-scattering-based lidar retrieval: method and results of cloud probing," *Appl. Opt.* **44**, 5565–5581 (2005).
 31. K. Sassen, "Dusty ice clouds over Alaska," *Nature (London)* **434**, 456 (2005).
 32. N. Sugimoto, Asian Dust Network, National Institute for Environmental Studies, Japan, available online at <http://info.nies.go.jp:8094/kosapub/index.html>(2005).
 33. T. Sakai, T. Nagai, M. Nakazato, Y. Mano, and T. Matsumura, "Ice clouds and Asian dust studied with lidar measurements of particle extinction-to-backscatter ratio, particle depolarization, and water-vapor mixing ratio over Tsukuba," *Appl. Opt.* **42**, 7103–7116 (2003).
 34. R. R. Draxler and G. D. Rolph, "HYSPLIT (HYbrid Single-Particle Lagrangian Integrated Trajectory) model access via NOAA ARL READY website," <http://www.arl.noaa.gov/ready/hysplit4.html>, NOAA Air Resources Laboratory, Silver Spring, MD (2003).
 35. S. A. Bowling and G. E. Shaw, "The thermodynamics of pollutant

removal as an indicator of possible source areas for arctic haze," *Atmos. Environ., Part A*. **26A**(16), 2953–2961 (1992).

36. G. E. Shaw, Geophysical Institute, University of Alaska, Fairbanks, AK Private Communication (2005).



Nathan L. Seldomridge received a BS degree in physics at North Park University, Chicago, in 2000, and an MS degree in electrical engineering from Montana State University, Bozeman, in 2005. He received a NASA Graduate Student Researchers Program (GSRP) fellowship, sponsored by the Stennis Space Center. His research activities include atmospheric measurements with lidar and passive radiometric imagers.



Joseph A. Shaw received a BS in electrical engineering from the University of Alaska—Fairbanks in 1987, an MS in electrical engineering from the University of Utah in 1989, and an MS and a Ph.D. in optical sciences from the University of Arizona in 1994 and 1996, respectively. He worked at the National Oceanic and Atmospheric Administration (NOAA), Environmental Technology Laboratory (ETL), in Boulder, Colorado, from 1989 to 2001, where he developed infrared spectro-radiometers and laser sensors for studying the Earth's atmosphere and oceans. In 2001, he joined the faculty of Montana State University, Bozeman, as an associate professor of electrical and computer engineering. Dr. Shaw is a Fellow of the Optical Society of America (OSA) and a member of SPIE.



Kevin S. Repasky received his BSEng degree in mechanical engineering from Youngstown State University in 1988 and his MS and PhD degrees in physics from Montana State University in 1992 and 1996, respectively. Currently, he is an assistant professor in the Electrical and Computer Engineering Department at Montana State University in Bozeman. His research activities are in the areas of laser source development and atmospheric remote sensing.

He has recently worked on external-cavity diode lasers, mode-locked fiber lasers, cw optical parametric oscillator (OPO) lasers, and cw Raman lasers.